

This is an Open Access document downloaded from ORCA, Cardiff University's institutional repository: <https://orca.cardiff.ac.uk/id/eprint/103452/>

This is the author's version of a work that was submitted to / accepted for publication.

Citation for final published version:

Guadix Montero, Susana, Alshammari, Hamed, Dalebout, Remco, Nowicka, Ewa, Morgan, David J., Shaw, Greg, He, Qian and Meenakshisundaram, Sankar 2017. Deactivation studies of bimetallic AuPd nanoparticles supported on MgO during selective aerobic oxidation of alcohols. *Applied Catalysis A: General* 546, pp. 58-66. 10.1016/j.apcata.2017.07.045

Publishers page: <http://dx.doi.org/10.1016/j.apcata.2017.07.045>

Please note:

Changes made as a result of publishing processes such as copy-editing, formatting and page numbers may not be reflected in this version. For the definitive version of this publication, please refer to the published source. You are advised to consult the publisher's version if you wish to cite this paper.

This version is being made available in accordance with publisher policies. See <http://orca.cf.ac.uk/policies.html> for usage policies. Copyright and moral rights for publications made available in ORCA are retained by the copyright holders.



Deactivation studies of bimetallic AuPd nanoparticles supported on MgO during selective aerobic oxidation of alcohols

Susana Guadix-Montero,^{a§} Hamed Alshammari,^{b§} Remco Dalebout,^{a,c} Ewa Nowicka,^{a,d} David J. Morgan,^a Greg Shaw,^a Qian He,^a Meenakshisundaram Sankar^{a*}

[a] *Cardiff Catalysis Institute, School of Chemistry, Cardiff University, Cardiff CF10 3AT, United Kingdom*

[b] *Chemistry Department, Faculty of Science, Ha'il University, P.Box 2440, 81451 Ha'il, Saudi Arabia*

[c] *Inorganic Chemistry and Catalysis, Debye Institute for Nanomaterials Science, Utrecht University, Universiteitsweg 99, 3584 CG Utrecht, The Netherlands*

[d] *Technical University Berlin, Straße des 17. Juni 124 10623 Berlin, Germany*

[§]Both authors have contributed equally to this paper

*Correspondence to Dr. Meenakshisundaram Sankar Tel: +44 29 2087 5748, Fax: (+44) 2920-874-030, E-mail: sankar@cardiff.ac.uk

Abstract

Here we report the synthesis and characterisation of high surface area MgO prepared *via* the thermal decomposition of various magnesium precursors (MgCO_3 , $\text{Mg}(\text{OH})_2$ and MgC_2O_4). Bimetallic gold-palladium nanoalloy particles were supported on these MgO materials and were tested as catalysts for the solvent-free selective aerobic oxidation of benzyl alcohol to benzaldehyde. All these catalysts were found to be active and very selective (>97%) to the desired product (benzaldehyde). However, MgO prepared *via* the thermal decomposition of magnesium oxalate displayed the highest activity among all the magnesium oxide supports tested. Attempts were made to unravel the reasons for the deactivation of these catalysts using different characterisation techniques namely *in situ* XRD, XPS, ICP-MS, TEM, and TGA-MS. From the data obtained, it is clear that MgO undergoes phase changes from MgO to $\text{Mg}(\text{OH})_2$ and MgCO_3 during catalyst preparation as well as during the catalytic reaction. Besides phase changes, strong adsorption of reactants and products on the catalyst surface, during the reaction, were also observed and washing the catalyst with organic solvents did not completely remove them. The phase change and catalyst poisoning were reversed through high temperature heat treatments. However, these processes led to the sintering of the metal nanoparticles. Moreover, substantial leaching of the support material (MgO) was also observed during the reaction. These latter two processes led to the irreversible deactivation of AuPd nanoparticles supported on MgO catalyst during the solvent-free selective aerobic oxidation of alcohols. Among the three different MgO supports studied in this article, an inverse correlation between the catalytic activity and Mg leaching has been observed. This article reports a deeper understanding of the mode of deactivation observed in metal nanoparticles supported on MgO during liquid phase reactions.

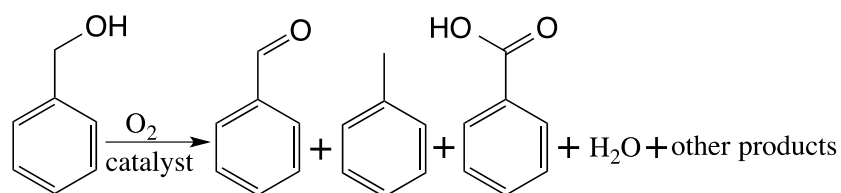
Keywords: High surface area MgO, supported AuPd nanoalloys, deactivation, leaching, selective oxidation, sintering.

Introduction

Selective aerobic oxidation is an important transformation not only in academic research but also in the industrial production of many fine and bulk chemicals.¹⁻⁵ It has been reported that this transformation alone is involved in approximately 25% of global organic chemical production and the worldwide market for this has been estimated to be close to \$50 billion.^{6, 7} Most of these oxidation reactions utilise undesirable stoichiometric oxidizing agents such as permanganates and chromates that produce environmentally unacceptable by-products. Hence, there is a need to design catalytic processes that use environmentally benign oxidants like such as, molecular O₂, or H₂O₂ that typically produce water as the only by-product.⁸⁻¹¹ However, the development of catalysts for such processes is extremely challenging, as most catalysts cannot activate oxygen efficiently enough without preserving high selectivity due to over-oxidation. Therefore, the design of an efficient catalyst with high activity, selectivity, and stability is highly desirable. A number of supported noble metal nanoparticles have been reported as catalysts for this reaction.^{1,12}

Benzyl alcohol is often used as a model compound for the selective oxidation of primary alcohols to aldehydes because of the challenges in producing and the importance of benzaldehyde.¹³⁻¹⁶ It is used to add almond flavour in cosmetics, scented products and food. In chemical industries, benzaldehyde is used as a precursor for producing many useful compounds ranging from pharmaceuticals to plastics. For example, malachite green (dye) is produced from benzaldehyde and dimethylaniline.¹⁷ A number of supported monometallic and bimetallic nanoparticles, typically Pt group metals, have been reported to be active for the solvent-free selective aerobic oxidation of benzyl alcohol to benzaldehyde.^{13, 18-21} However, during this reaction, toluene, benzoic acid, benzyl benzoate and benzene are formed as by-products lowering the selectivity to benzaldehyde.²²⁻²⁴ Typically, benzoic acid, benzylbenzoate, and benzene are formed in smaller quantities (*ca* <5%). During this reaction, toluene is also formed in a substantial amount (*ca* 20%). Production of toluene has to be suppressed through catalyst design in order to increase the selectivity of benzaldehyde. Toluene is formed by the disproportionation of 2 moles of benzyl alcohol into an equimolar mixture of benzaldehyde and toluene, and occurs along with the oxidative dehydrogenation of benzyl alcohol to benzaldehyde.²² After extensive kinetic and mechanistic

investigations on these two reactions, we found that the active site for the oxidative dehydrogenation reaction is the (bi)metallic sites and that for the disproportionation reaction is the metal-support interface.^{22,25} We have further demonstrated that by tuning this metal-support interface, using basic supports such as MgO or ZnO, we can switch-off the disproportionation reaction and thereby the toluene production.^{23,25} The basicity of MgO in supported metal catalysts has been exploited for the homogeneous base-free oxidation of bioderived polyols.^{26, -29}



Scheme 1. Schematic representation of the catalytic solvent-free, aerobic oxidation of benzyl alcohol.

Several research groups have reported the catalytic activities of metal nanoparticles supported on MgO for many reactions including CO oxidation, base-free oxidation and hydrogenation/hydrogenolysis of bioderived platform molecules, oxidative esterification of alcohols, and more.³⁰⁻³³ MgO, on its own, has been reported to be an efficient solid-base catalyst for coupling and transesterification reactions.³⁴⁻³⁶ Recently we have reported the one-pot synthesis of “*raspberry ketone*” from 4-methoxy benzyl alcohol and acetone using AuPd/MgO catalyst, where MgO catalyses the aldol condensation reaction between 4-methoxy benzyl alcohol and acetone.³⁷ In all these reactions, the basicity of MgO has been exploited for the catalytic reaction. The basicity of MgO is believed to be the result of the presence of Mg²⁺-O²⁻ ion pairs in different coordination environments.³⁴ Several studies show that the strongest basic sites are located at the low coordination sites such as defects, corners, edges, or on high Miller index surfaces. These sites, hence the basicity of MgO, are very sensitive to the preparation route.³⁸

In supported metal catalyst systems, the catalytically active sites are metallic sites, metal-support interfacial sites, and the support sites. In the case of supported bimetallic

AuPd catalysts, the activities of bimetallic sites have been tuned by optimising the size, composition, and nanostructure through appropriate synthesis strategies.³⁹ The metal-support interfacial sites have been tuned by choosing different supports thereby enhancing the selectivity during aerobic oxidation of benzyl alcohol.²³ Here, we attempt to optimise the support properties for the AuPd/MgO catalyst and study its effects on the resultant catalytic activity and stability. In order to achieve that, we prepared a variety of MgO materials from different precursors and used them as supports for 1% AuPd/MgO catalyst. A number of metal nanoparticles supported on MgO have been reported for several reactions including liquid phase reactions, however, the stabilities of these catalysts have not been studied in detail. Hence, another important objective of this work is to study the stability and mode(s) of deactivation of AuPd/MgO catalyst during the liquid-phase, solvent-free, selective aerobic oxidation of benzyl alcohol.

Experimental

Preparation of high surface area MgO

Three high surface area MgO materials were prepared from the following magnesium precursors: MgCO₃, Mg(OH)₂ and MgC₂O₄ *via* previously reported methods.⁴⁰ The resultant high surface area materials were denoted as MgO(1), MgO(2), and MgO(3) respectively. Briefly, the high surface MgO materials were prepared as follows:

MgO(1): 25 g of MgCO₃ (Sigma Aldrich) was stirred in 750 mL of deionised water at 70 °C for 30 min. The resulting solid was filtered, dried at 90 °C for 24 h and then calcined at 450 °C (heating ramp: 10 °C min⁻¹) in static air for 2 h.

MgO(2): Commercial Mg(OH)₂ (Sigma Aldrich) was calcined at 600 °C (heating ramp: 10 °C min⁻¹) in static air for 2 h. Following this heat treatment, the resultant MgO (10 g) was rehydrated by refluxing it in deionised water (125 mL) for 3 h. The resultant solid was filtered, dried at 90 °C for 24 h and then calcined at 450 °C (heating ramp: 10 °C min⁻¹) in static air for 2 h.

MgO(3): This MgO was prepared by the calcination of magnesium oxalate. Magnesium oxalate (MgC₂O₄) was prepared using a method reported by Putanov *et al.*⁴¹ An aqueous solution of magnesium acetate was prepared by dissolving 26.8 g of Mg(CH₃COO)₂·4H₂O (Sigma Aldrich) in 25 mL of deionised water. An aqueous

solution of $\text{H}_2\text{C}_2\text{O}_4 \cdot 2\text{H}_2\text{O}$ (Sigma Aldrich) was also prepared by dissolving 16.5 g of it in 100 mL of deionised water separately. In a 250 mL round-bottom flask, the magnesium acetate solution was stirred at 40 °C and to that the oxalic acid solution was added dropwise while stirring over a period of 1 h. The resultant precipitate of magnesium oxalate was filtered, dried at 90 °C for 24 h and then calcined at 450 °C (heating ramp: 10 °C min⁻¹) in static air for 2 h.

MgO(C): Commercial magnesium oxide (light) was purchased from BDH and used as it is without any further heat treatment.

All these support materials were used for the catalyst preparation without any further modification.

Catalyst preparation

Bimetallic AuPd nanoalloys were supported on MgO supports *via* sol immobilization and modified impregnation methods and the detailed experimental procedures are reported elsewhere.^{23, 26, 42}

Sol immobilisation

In a typical procedure, 1 wt. % of AuPd/MgO (molar ratio of Au vs Pd is 1) catalyst was prepared by using aqueous solutions of the metal precursors [PdCl_2 (99%, Sigma Aldrich) and $\text{HAuCl}_4 \cdot 3\text{H}_2\text{O}$ (>99.9%, Sigma Aldrich)] with a metal concentration of 6 mg_{Pd} mL⁻¹ and 12.5 mg_{Au} mL⁻¹, respectively. This catalyst is called as 1% AuPd/MgO further in this article. The requisite volumes of gold and palladium precursor solutions were added to 800 mL deionised water and stirred for 15 min before addition of aqueous polyvinyl alcohol (PVA, Sigma Aldrich, Mw=10000, 80% hydrolysed) solution (1 wt.% solution). The solution was further stirred for 15 min. A freshly prepared aqueous solution of sodium borohydride (0.1 M, $\text{NaBH}_4/(\text{Au}+\text{Pd}) = 5$ (molar ratio)) was quickly added to the above mixture to form a dark brown sol. The mixture was stirred for an extra 30 min until addition of the support (MgO, 1.98 g for a 2 g catalyst batch). The final slurry was stirred for 1 h for complete immobilisation. Subsequently, the catalyst was recovered by filtration, washed with 2 L of deionised water, and dried at 110 °C overnight. This catalyst was used in the reaction without any modification and it was labelled as S_{Im} catalyst.

Modified impregnation method

1 wt.% AuPd/MgO catalyst with equal weight loadings of the two metals (i.e. 0.5wt% Au & 0.5wt%Pd) was prepared using a modified impregnation method. An aqueous solution of PdCl₂ (99%, Aldrich) was prepared with a metal concentration of 6 mg_{Pd} mL⁻¹ in a 0.58 M HCl solution. An aqueous solution of HAuCl₄.3H₂O (>99.9%, Aldrich) with a metal concentration of 12.5 mg_{Au} mL⁻¹ was also prepared separately. Requisite amounts of metal precursor solutions were added to a 50 mL round-bottom flask fitted with a magnetic stirrer bar. Additional volume of deionised water was added to make the total volume of the impregnation mixture to 16 mL. The solution was stirred vigorously and the temperature of the solution was increased from room temperature (27 °C) to 60 °C. At 60 °C, the MgO support (1.98 g) was added slowly over a period of 15-20 min with constant vigorous stirring. The slurry was stirred at 60 °C for an additional 15 min, followed by an increase in temperature to 95 °C and the slurry was stirred until full water evaporation (typically 16 h). Subsequently, the resultant dry powder was ground thoroughly and reduced at 400 °C under a flow of 5 vol% H₂/Ar (4 h, 10 °C min⁻¹). This catalyst was labelled as M_{Im} catalyst.

Catalyst testing

The catalytic activities of 1% AuPd/MgO catalysts were tested in a 50 mL glass, stirred Radleys® carousel reactor for the solvent-free liquid phase oxidation of benzyl alcohol with oxygen. In a typical reaction, 20 mg of the catalyst was suspended in 2 g of the substrate without any additional solvent. The reaction mixture was stirred at 1000 rpm with a constant inlet pressure (1 barg) of pure oxygen. At the end of the reaction, the reactor was cooled in an ice bath until the temperature of the reaction mixture reaches below 5°C. After de-pressuring the reactor, the catalyst was removed by centrifugation. An aliquot of the clear liquid reaction mixture along with a fixed amount of internal standard (*o*-xylene) was injected in a GC (Agilent 7820A) fitted with a Agilent J&W HP-5 GC column and a flame ionization detector. Quantitative analyses of the substrates and products were performed with the help of calibration plots and response factors. For reusability studies, after the end of the reaction, the catalysts were filtered, washed with acetone several times, and dried in an oven at 120 °C for overnight. These dried catalysts were calcined at 450 °C in static air for 4 h and used for the next reaction.

The catalytic results are within an error limit of $\pm 5\%$ (determined from 5 separate catalytic experiments).

Catalyst Characterisation

Powder X-ray diffraction studies

In situ and *ex situ* powder X-ray diffraction (XRD) of MgO materials and 1% AuPd/MgO catalysts were performed using a PANalytical® X'Pert PRO apparatus. The X-rays were generated by a copper anode ($K\alpha$ 1.54184 Å). The samples were scanned between a 2θ angle of 10 and 80° with a step size of 0.017 or 0.008° for the *in situ* and *ex situ* measurements, respectively. The *ex situ* measurements were performed at 25 °C, whereas the diffraction profiles for the *in situ* measurements were recorded between 25 and 700 °C in static air with a heating rate of 10 °C min⁻¹.

Surface area measurements

Surface area of the supports and catalysts were measured by nitrogen physisorption at -196 °C using a Quantachrome Nova instrument. Surface areas were calculated according to the Brauner Emmet Teller (BET) method over a P/P_0 range where a linear relationship was maintained. All samples were degassed under N₂ at 110 °C for 2 h to remove adsorbed water molecules prior to the analysis.

TGA & TGA-MS analyses

TGA experiments for different MgO materials were obtained using a TA Instruments Ltd SDT Q600 thermal analysis machine under the flow of air. In another set of experiments, fresh and spent 1% AuPd/MgO catalysts were characterised using a thermogravimetric analyser fitted with a mass spectrometer (TGA-MS) under an oxidising atmosphere. These later experiments were performed on a PerkinElmer Pyris 1 thermogravimetric analyser connected to a Clarus® SQ 8S mass spectrometer. Under an air flow of 30 mL min⁻¹ the sample was stabilised at 30 °C for 20 min. After stabilisation the temperature was increased to 800 °C at a rate of 10 °C min⁻¹. No corrections for gas buoyancy effects were applied. For the MS data analysis the m/z ratios of molecular ion peaks of probable decomposition products are followed. Specifically, 18 - H₂O, 44 - CO₂, 78 - benzene (PhH), 91 - toluene (PhCH₃), 106 -

benzaldehyde (PhCHO), and 108 - benzyl alcohol (PhCH₂OH) were followed. In this article only the relative intensities are reported.

Inductively Coupled Plasma-Mass Spectroscopic (ICP-MS) studies

Metal contents in catalysts, product solutions, and stock solutions for catalyst preparation were analysed and quantified by inductively coupled plasma-mass spectrometry (ICP-MS) on an Agilent 7900 ICP-MS with I-AS auto sampler with Platinum Sampling and Skimmer cones, concentric nebulizer and quartz double pass spray chamber. 2.5 mm ID torch for aqueous analysis of Pd and Au, 1.5 mm ID torch for analysis of Mg. All analysis was run using helium (He mode) and the ORS cell to reduce interferences. For metal content determination in solids, *ca.* 2 mg of catalyst was dissolved in 10 mL aqua-regia for at least 12 h. The final solution was diluted to 50mL with water in a volumetric flask. In all cases, further dilutions were done if required. All results were done in duplication and further analyses were performed if two results differed.

For the analysis of Mg in reaction mixture auto-sampler was not used, sample aspirated manually using natural uptake through sampling probe. 20 % ArgOx is added to burn off carbon from organic solvent at 10% of the carrier gas which was set at 0.85l/min RF power 1600W, RF Matching 1.7 Sample Depth 10mm. Calibration carried out using Agilent Multi-Element calibration standard 2A (p/n 8500-6940) made up in MeOH at 2, 1, 0.5, 0.1 and 0 mg/l. Samples were diluted in MeOH (x5000 and x50 as per supplied report) to bring them within calibration range and to reduce matrix effects of high Mg concentration and match calibration matrix to subsequent sample matrices as closely as possible. Analyses were carried out using standard addition techniques using the first sample (on the supplied report) as calibrant, which is then converted by the instrument software into an external calibration for subsequent samples.

X-ray Photoelectron Spectroscopic (XPS) studies

Elemental analysis and atom oxidation states of the AuPd/MgO catalyst surfaces were performed on a Thermo ScientificTM K-Alpha⁺ X-ray photoelectron spectrometer (XPS) utilising monochromatic Al radiation operating at 72 W power at a spot size of 400 microns. Dual low energy electron and Ar⁺ neutralisation was used and all data calibrated to the C(1s) line at 284.8 eV when required. All data was analysed using

CasaXPS using Scofield sensitivity factors corrected with an energy dependence of 0.6, after application of a Shirley background.

Transmission Electron Microscopic (TEM) studies

Metal particle size analyses of the 1%AuPd/MgO catalysts were performed on a Transmission electron microscope (JEM-2100F (JEOL)). Prior to the TEM analysis, samples were dispersed with ethanol under ultrasonication. Supernatant liquid was dropped on a Ni grid and dried overnight before analysis.

Scanning Electron Microscopic studies:

Scanning EM imaging and X-ray analysis were carried out using TESCAN MAIA3 in Cardiff University, also equipped with Oxford Instrument SDD Detector X-Max^N 80 T. The SEM-EDX mapping was carried out and analysed using AZtec software by Oxford Instrument.

Results and discussion

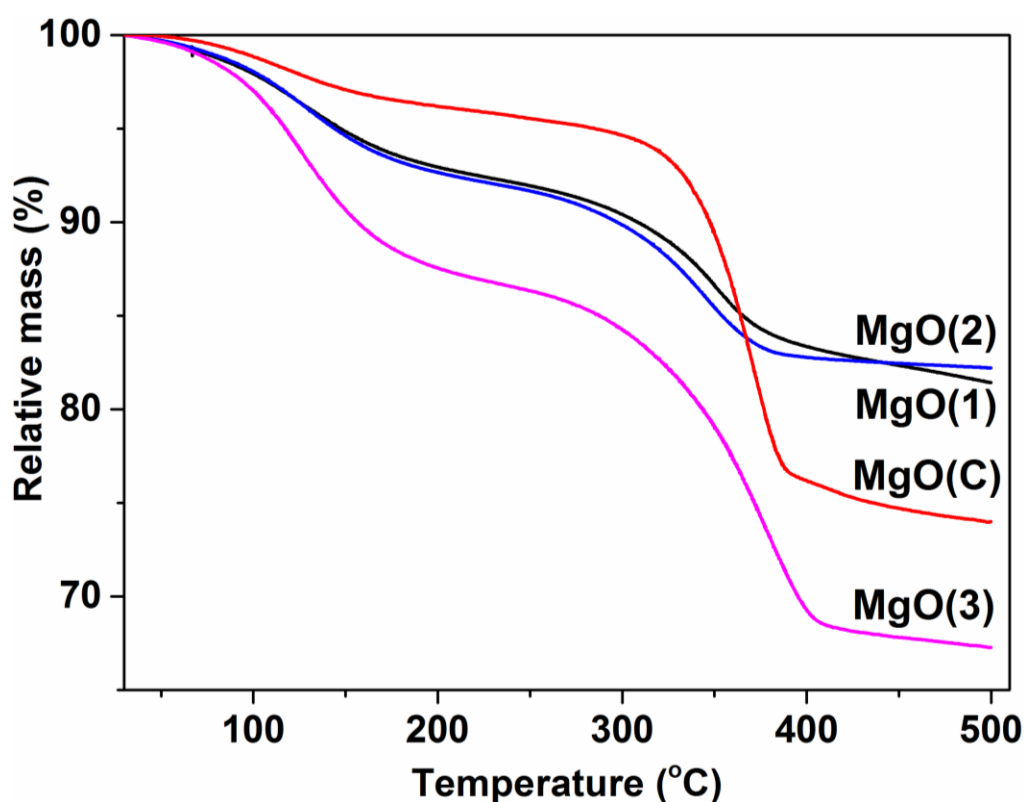


Figure 1: TGA curves of different MgO materials

MgO has been widely used as a support material for metal nanoparticles to be used as catalysts for many reactions including selective oxidation reactions.^{32,33,43} Specifically, AuPd/MgO catalyst has been reported to be very selective for the aerobic oxidation of primary alcohols and polyols.^{23, 26} To study the role of the properties of MgO in this catalyst, we prepared different types of MgO from different precursors. MgO(1) from MgCO₃, MgO(2) from Mg(OH)₂ and MgO(3) from MgC₂O₄. The resultant MgO materials are reported to have high surface areas (typically between 200 – 300 m²g⁻¹).⁴⁰ For comparison, commercial MgO (MgO(C) from BDH) was also used as a support. The TGA of all MgO materials (Figure 1) indicate the removal of varying quantities of CO₂ and H₂O during the heat treatments. It has been previously reported that water is lost between 250 and 400 °C and CO₂ removal occurs between 325 and 500 °C.⁴⁴ This is further proved by the TGA-MS of MgO(3), where CO₂ and H₂O are removed between 350 and 450 °C (supporting information Figure S1) The powder XRD patterns of all these materials (Figure 2) show that MgO(1), MgO(2) and MgO(3) have cubic periclase (MgO) phase with crystallite sizes between 45 – 60 Å (calculated using Debye-Scherrer equation). The MgO(C) sample displayed reflections from both MgO and Mg(OH)₂ phases.⁴⁴ However, TGA results (Figure 1) show that all samples contain CO₂ and H₂O. This suggests that in MgO(1), MgO(2) and MgO(3) materials, the Mg(OH)₂ and MgCO₃ phases are highly amorphous and/or highly dispersed whereas in the commercial sample the Mg(OH)₂ phase is crystalline. BET surface areas of all the MgO samples were found to be high (220 – 280 m²g⁻¹) (Table 1).

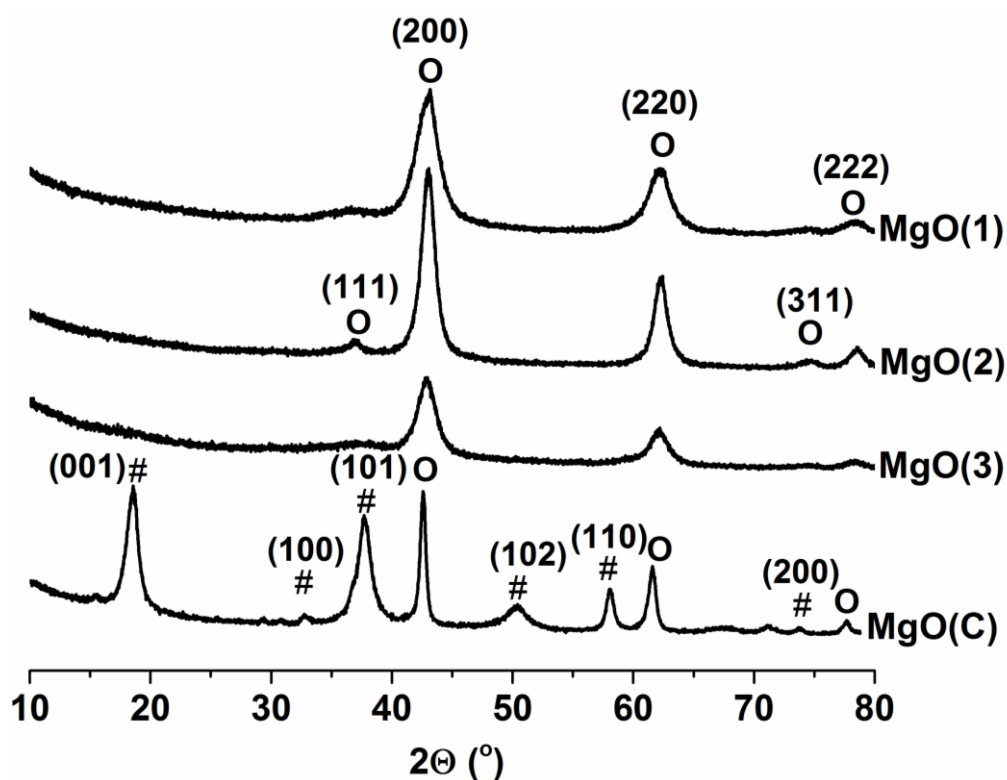


Figure 2: The powder XRD patterns of MgO(C), MgO(3), MgO(2) and MgO(1). Key: o denotes indexed reflections corresponding to periclase MgO and # denotes reflections from Mg(OH)₂.

Table 1: Surface area of different MgO materials and supported AuPd catalysts.

Support Material	Crystallite Size ^a Å	S _{BET} (m ² g ⁻¹)	
		Support	1% AuPd/MgO
MgO (1)	47	267	ND
MgO (2)	60	237	53 ^b
MgO (3)	55	283	73 ^b /69 ^c
MgO (C)	167	228	87 ^b

a: Calculated using Debye-Scherrer equation, b: catalyst prepared via sol immobilisation method, and c: catalyst prepared via modified impregnation method.
ND : not determined

Bimetallic AuPd nanoalloys were supported on different MgO materials *via* sol immobilization and modified impregnation techniques.^{42, 45} These two methods have been reported to be very effective for the synthesis of active AuPd/MgO catalysts.^{25, 46} The sol immobilization technique is the preferred method of preparing supported AuPd nanoalloy catalysts with precise control over the particle size, whereas the modified impregnation technique is preferred for controlling the metal particle size as well the composition of the bimetallic particles.⁴⁷ 1% AuPd/MgO(3) prepared by both techniques have been tested for the solvent-free, aerobic oxidation of benzyl alcohol (see supporting information Figure S2). Both catalysts (M_{im} and S_{im}) have been found to be equally active for the aerobic oxidation of benzyl alcohol and the selectivity for benzaldehyde has always >97%. The surface areas of MgO materials reduced substantially upon loading of AuPd nanoparticles (Table 1) because of the re-dispersion and drying processes involved during the catalyst synthesis.

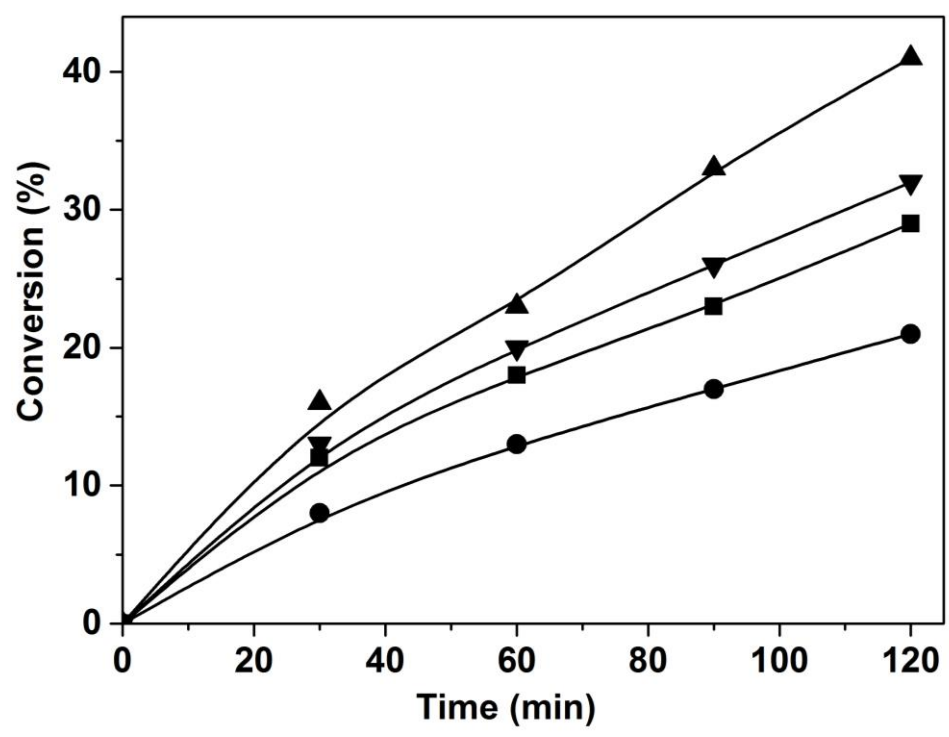


Figure 3: Reaction profile of solvent-free, aerobic oxidation of benzyl alcohol over AuPd supported on different MgO materials prepared by sol immobilisation technique. Reaction conditions: catalyst: 0.02 g; pO₂: 1 barg; benzyl alcohol: 2 g; T: 120 °C. (Key: ●: AuPd/MgO(2); ■: AuPd/MgO(1); ▼: AuPd/MgO(C) & ▲: AuPd/MgO(3)). In all these reactions, the selectivity for benzaldehyde was found to be >97% and the remaining products include toluene, benzyl benzoate, and benzoic acid.

Since both methods resulted in catalysts with comparable activities, we decided to perform further studies using S_{Im} catalysts only, unless specified. We prepared different 1% AuPd/MgO catalysts using MgO(1), MgO(2), MgO(3) and MgO(C). All these catalysts were tested for the solvent-free selective aerobic oxidation of benzyl alcohol and activity profiles of all the catalysts are presented in Figure 3. The activity follows the order 1% AuPd/MgO(2) < 1% AuPd/MgO(1) < 1% AuPd/MgO(C) < 1% AuPd/MgO(3). All these catalysts showed excellent selectivity for benzaldehyde (typically >97%) and other products such as toluene, benzoic acid, and benzyl benzoate were detected with a combined selectivity of <3%. Among the catalysts tested, 1% AuPd/MgO(2) is the least active catalyst giving 21% conversion after 2 h of reaction time. However, under identical reaction conditions, 1% AuPd/MgO(3) catalyst gave 41% conversion. This nearly 2-fold increase in the catalytic activity was achieved by tuning the synthesis strategy of the support material. Although in supported metal catalysts, most support materials are typically inert and these results indicate that they can actively influence the catalytic activity of the material, either directly or indirectly. The most active 1% AuPd/MgO(3) catalyst has also been found to be moderately active for the solvent-free aerobic oxidation of 1-octanol to 1-octanal (see supporting information Figure S3). It is important to note that aliphatic alcohols such as 1-octanol are inherently less active than benzylic alcohols.

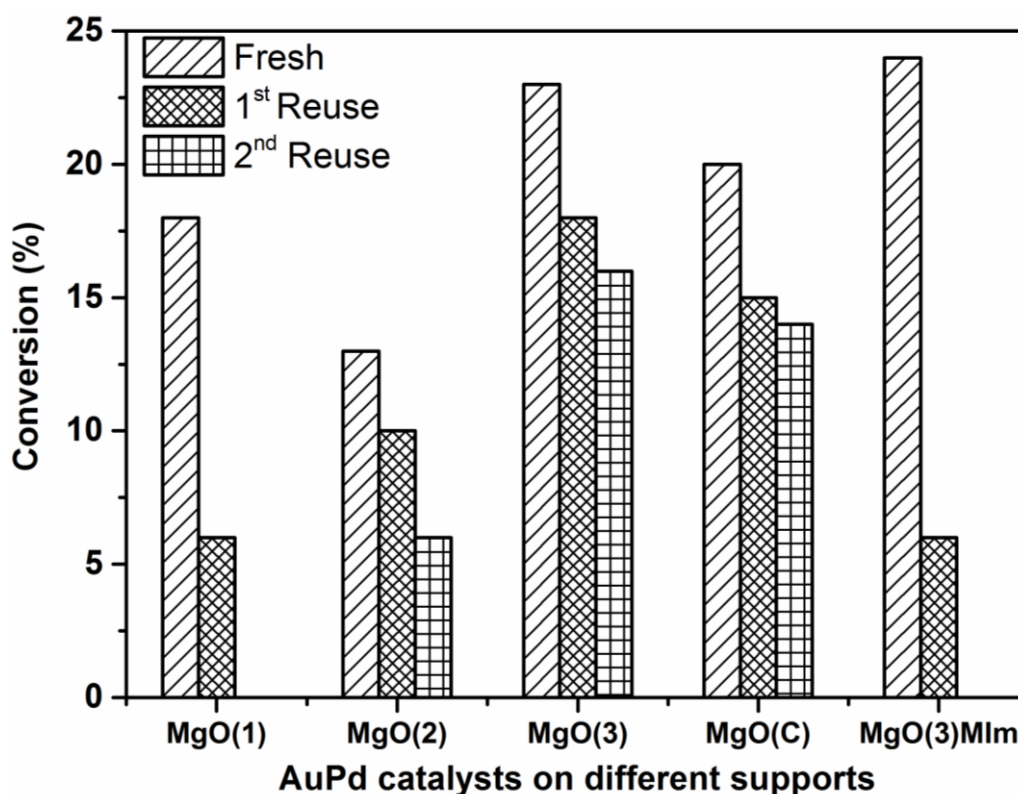


Figure 4: Reusability data for 1%AuPd/MgO(1), 1%AuPd/MgO(2), 1%AuPd/MgO(3), 1%AuPd/MgO(C) and 1%AuPd/MgO(3)-M_{Im} catalysts. Reaction conditions: catalyst: 0.02 g; pO₂: 1 barg; benzyl alcohol: 2 g; T: 120 °C; time: 1 h.

Next we investigated the reusability of these active and selective catalysts, which is an important property of heterogeneous catalysts. For this study, the catalysts were separated from the reaction mixture after the end of the reaction, washed with acetone and dried overnight in an oven at 120 °C. Then the dried catalysts were calcined at 450 °C under static air for 2 h and used for the 1st reuse experiment. The catalyst recovered from this 1st reuse reaction was treated similarly for the 2nd reuse data. The reusability data, presented in Figure 4, clearly indicate that all the catalysts tested deactivated at the end of the reaction. Common reasons for the deactivation of supported metal catalysts could be assigned to (a) leaching of active metal component, (b) sintering of metal nanoparticles, and/or (c) irreversible adsorption of products (poisoning).⁴⁸ Understanding the mode of deactivation of these catalysts is crucial to the design reactivation strategies.^{48,49} For all the following studies, we used 1% AuPd/MgO(3)-S_{Im} catalyst since it is the most active catalyst among all the catalysts tested.

To study the role of adsorbed reactants and/or products on the deactivation of 1%AuPd/MgO(3), the fresh and recovered catalysts were characterised using TGA-

MS. The results, presented in Figure 5, indicate that products such as toluene, benzaldehyde, benzene, and benzoic acid were adsorbed on the catalyst after the reaction (Figure 5b). Thorough washing the spent catalyst with acetone did not remove these strongly adsorbed products. The adsorbed compounds including CO₂ and H₂O constitute nearly 63% of the mass of the spent catalyst. Upon heating at 110 °C toluene, benzaldehyde and benzene are removed, indicating that these compounds are not strongly adsorbed. Around 300 °C, water and CO₂ are removed and this is similar to the fresh 1% AuPd/MgO(3) catalyst though at a slightly lower temperature (Figure 5a). Remaining compounds such as CO₂, benzene, benzyl alcohol, and benzaldehyde are removed between 400 and 600 °C. The CO₂ and benzene generated in this temperature zone originate from the decomposition of benzoic acid and benzaldehyde, respectively. Benzene is formed by the decarbonylation of benzaldehyde and CO₂ is produced by the decarboxylation of benzoic acid to benzene. In addition to these products, H₂O is also removed at these temperatures, which suggests combustion of organic compounds. A few other compounds were also detected by the mass spectrometer, however their corresponding peaks are not presented in Figure 5b for clarity. These compounds are not related to the reactants or products of this reaction as they were formed by the decomposition of PVA, the stabiliser ligand used in the catalyst synthesis.

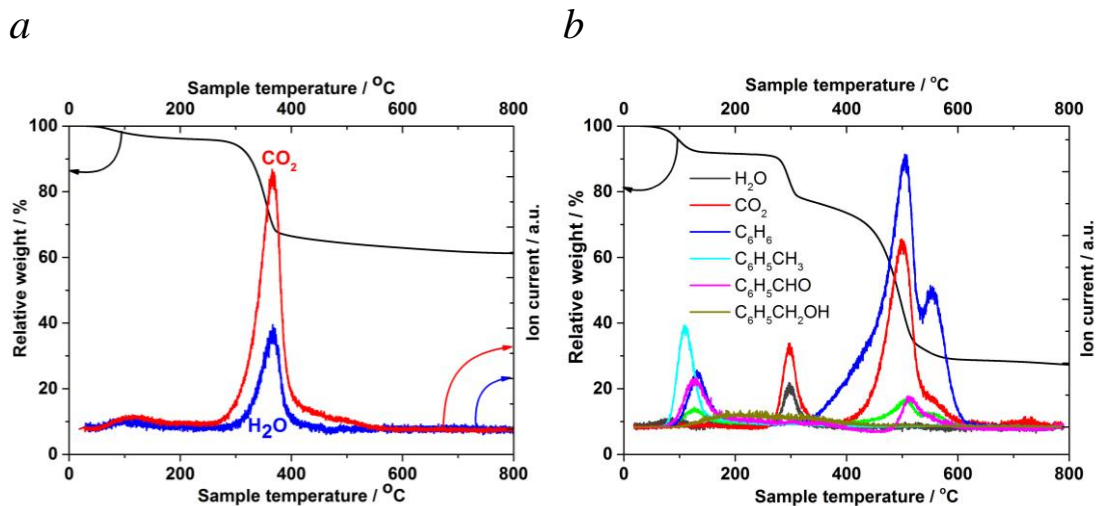


Figure 5: TGA-MS of 1%AuPd/MgO(3) fresh (a) and 1%AuPd/MgO(3) used (b) under oxidation atmosphere. Some mass peaks detected in 1%AuPd/MgO used catalyst have been omitted for clarity.

The presence and removal of CO₂ and H₂O from the support material prompted us to further study the phase transformations of both 1% AuPd/MgO(3) fresh and 1% AuPd/MgO(3) spent catalysts using *in situ* XRD at different temperatures starting from 25 up to 700 °C under both oxidising and inert atmospheres at a heating rate of 10 °C min⁻¹ (Figure 6). XRD patterns of the catalysts were recorded after every 50 °C raise in temperature.

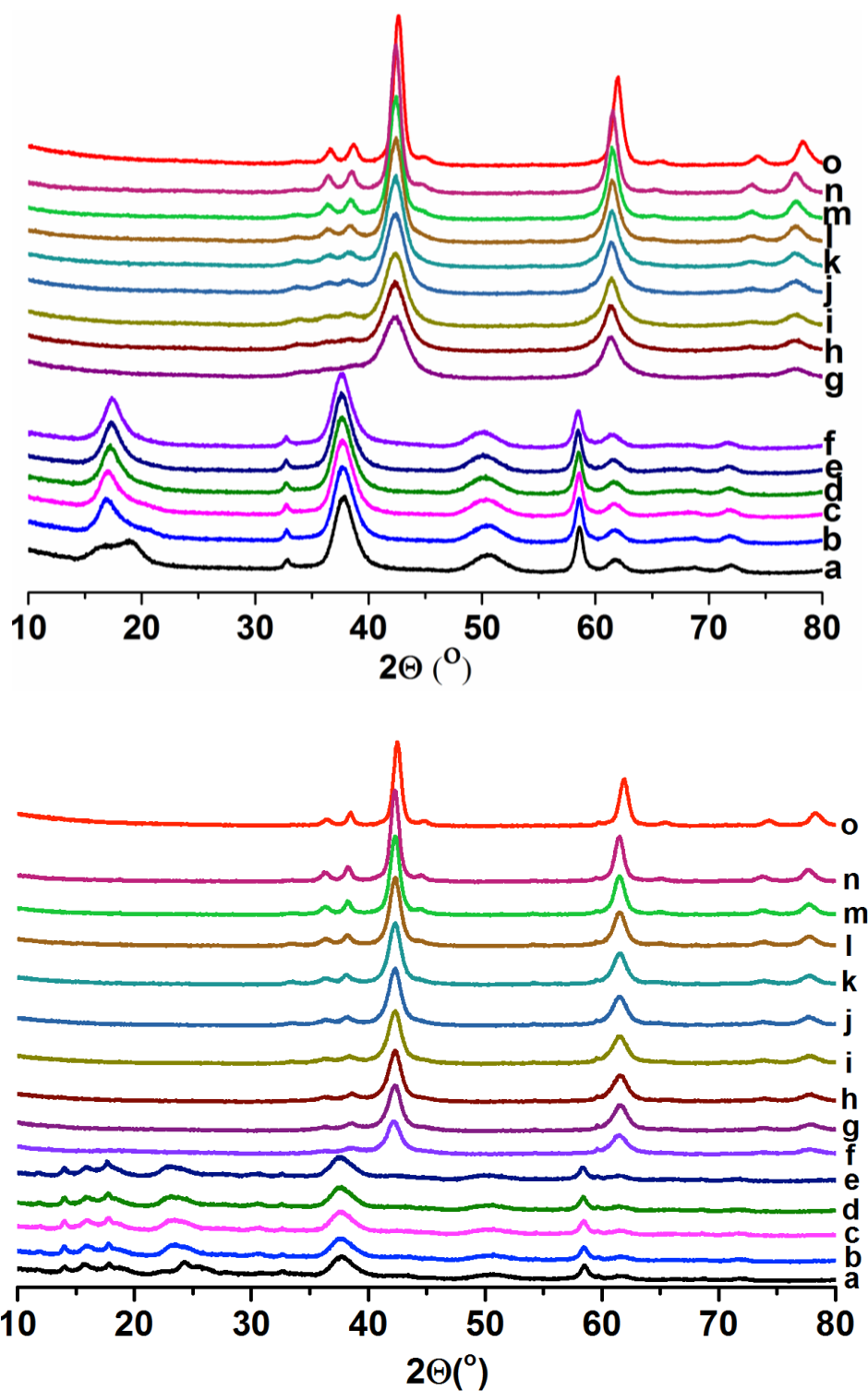


Figure 6: In situ XRD of 1%AuPd/MgO(3) fresh (top) and 1%AuPd/MgO(3) used (bottom). XRD patterns of the materials at different temperatures under static air. (a) XRD pattern of 1%AuPd/MgO(3) at 25 °C and then each pattern was recorded after raising the temperature of the catalyst by 50 °C with temperature starting from 100 °C

(b) until 700 °C (n). (o) XRD pattern recorded at 50 °C after treating the catalyst at 700 °C.

The support materials in both fresh and spent catalysts at 25 °C were predominantly Mg(OH)₂, as evidenced by the reflections at 2θ 17° (001), 38° (101) and 58° (110), because of the method of immobilizing AuPd nanoalloys involving a large volume of water. However, the support in both samples transforms to MgO at 300 °C for the spent catalyst (Figure 6 bottom) and at 350 °C for the fresh catalyst (Figure 6 top). This data correlates well to the TGA-MS data presented in Figure 5. Above 350 °C the materials became more crystalline with the increase in temperature as evidenced by sharper peaks in the XRD patterns. A similar behaviour is also observed for the pure MgO(3) material (see supporting information Figure S4). For the used catalyst, some tiny unassigned reflections were observed at room temperature, however they disappeared above 300 °C, indicating that they may be as a consequence of a portion of adsorbed reaction products. Reflections from Au and Pd were not visible due to low loading and small particle size. TGA-MS and *in situ* XRD results indicate that the adsorbed products and phase transformation of MgO(3) could be a major reason for the deactivation of the 1% AuPd/MgO(3) catalyst. However, this can be reversed by heating the sample at temperatures above 400 °C.

For the reusability studies, presented in Figure 4, we calcined the catalysts at 450 °C for 2 h, thereby removing all the adsorbed organics as well as transforming the Mg(OH)₂ phase to MgO phase. However, the spent catalysts were still found to be less active than the corresponding fresh catalysts. Next, we studied the leaching of metal components in the reaction mixture using ICP-MS. The results presented in Figure 7 indicate that the reaction mixture contained lesser amounts of Au and Pd, however there is substantial leaching of Mg for all the catalysts. There is a trend in the amount of Mg leaching. 1% AuPd/MgO(3)-SIm showed the least Mg leaching whereas the catalyst 1% AuPd/MgO(2)-SIm showed maximum Mg leaching (ca 67%). This Mg leaching trend correlates well with the observed catalytic activities (Figure 7). The catalyst with maximum leaching (1% AuPd/MgO(2)) showed least activity whereas the catalyst with minimum leaching showed the maximum activity (1% AuPd/MgO(3)). Because of substantial leaching, the AuPd bimetallic sites may not be able to retain their original particle size and nanostructure. One of the products, benzoic acid, could be one of the reasons for MgO leaching. We further tested the leaching for 1% AuPd/MgO(3) M_{Im}

catalyst and found substantial Mg leaching (data not presented here). This indicates that leaching of MgO is because of the nature of the support rather than the method of supporting AuPd nanoparticles on MgO (*i.e.* sol immobilisation *vs* modified impregnation). It is important to highlight that the sol immobilisation method involves only drying (at 120 °C), whereas the modified impregnation method involves high temperature gas phase reduction (at 400 °C for 4 h)

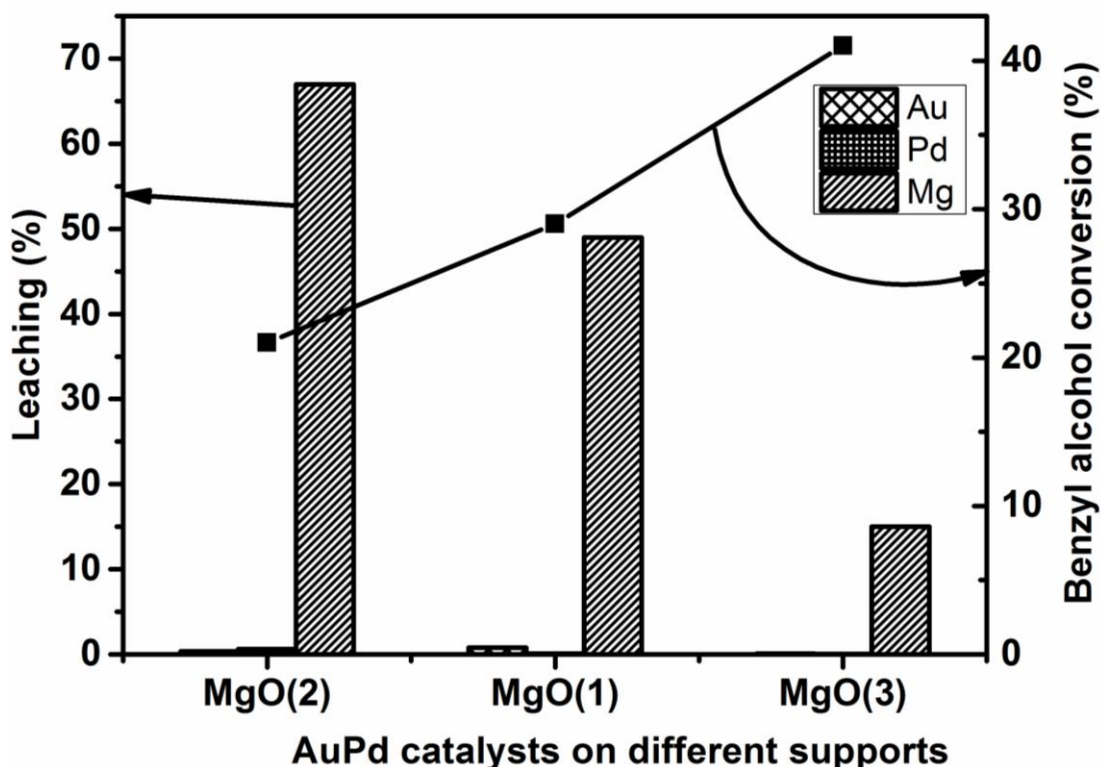


Figure 7: Correlation of catalyst components leaching with the catalytic activity for 1%AuPd/MgO(1), 1%AuPd/MgO(2) and 1%AuPd/MgO(3). The leached catalyst components were quantified using ICP-MS of the reaction mixture after 2 h of catalytic reaction at 120 °C. The benzyl alcohol conversion values are from Figure 3 (2 h data). The % leaching was calculated based on the amount of metal components present in the catalyst (0.02 g) taken for the reaction (through ICP-MS of the fresh catalyst) and the amount of metal components present in the reaction mixture determined by ICP-MS.

Fresh and spent AuPd supported on MgO(1), MgO(2) and MgO(3) catalysts were characterised by transmission electron microscopy (TEM) and the data are presented in Figure 8 (a-f). It is clear that there is no apparent particle size difference between the three fresh catalysts (Figure 8a-c). This is not unexpected because of the method of

preparation of all these catalyst *i.e.* sol immobilisation. In this methodology, the procedure is identical till the addition of support. The bimetallic sol is prepared before the addition of support. Hence it is not surprising that all the catalysts have almost similar particle size. The change of the nature of MgO support can be also observed from TEM characterisation. As shown in Figure 8, the MgO in the fresh AuPd/MgO(3) and AuPd/MgO(2) catalysts have a “flake-like” morphology, evidenced by the curled edge features (highlighted using white arrows) in Figure 8 (b & c). In contrast, after the 1st reuse (Figure 8(e & f)), those features in the MgO support disappeared, suggesting that the MgO has been significantly modified during the reaction. This is consistent with the TGA-MS & XRD characterisation results shown above (Figure 5 & 6). We also observed signs of particle agglomeration, for AuPd/MgO(3) (Figure 8(f)), which is also partially responsible for the deactivation. For this catalyst, the particle size agglomeration is more prominent after 2nd reuse (supporting information Figure S5). In the cases of AuPd/MgO(1) and AuPd/MgO(2) the metal particles sizes appear to be the same indicating less agglomeration in these catalysts.

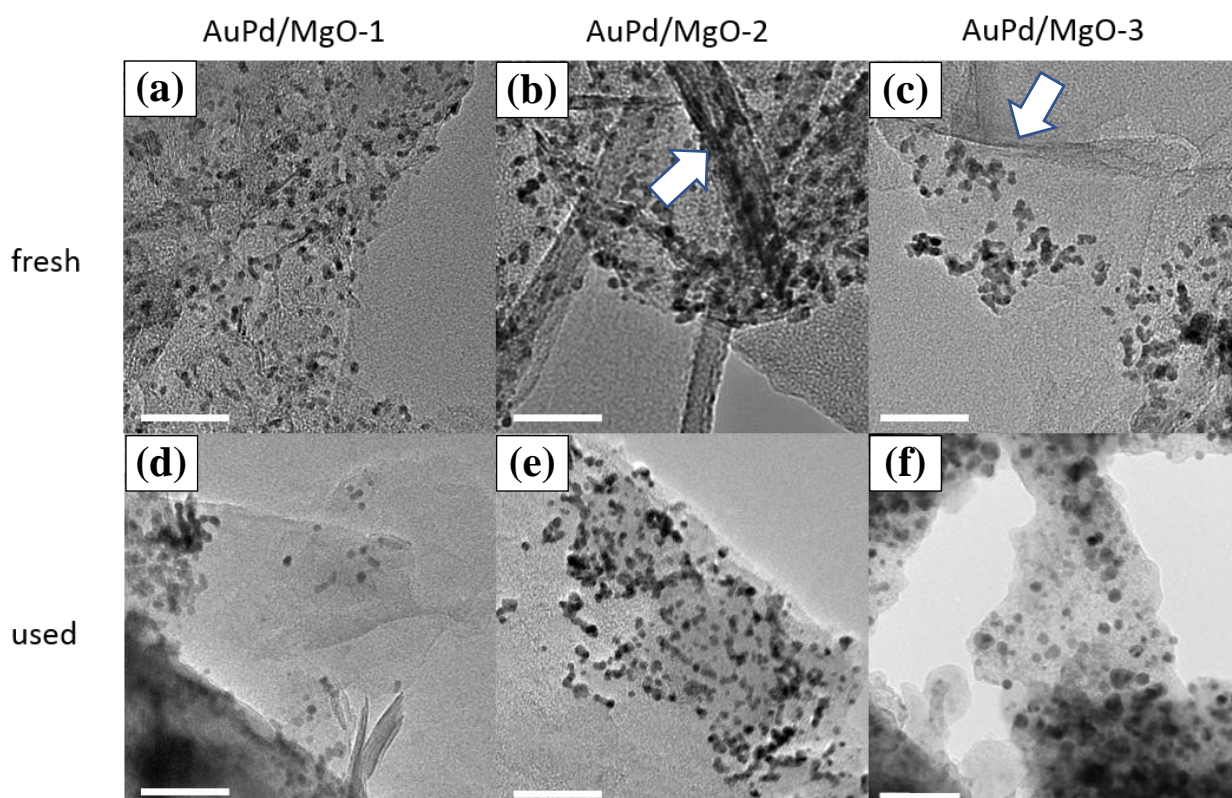


Figure 8: Top row: TEM bright field images of fresh (a) AuPd/MgO(1), (b) AuPd/MgO(2) and (c) AuPd/MgO(3) catalysts. Bottom row: TEM bright field images of the catalyst after 1st Reuse (d) AuPd/MgO(1), (e) AuPd/MgO(2) and (f) AuPd/MgO(3). The MgO supports are “flake-like” in the fresh catalyst, evidenced by many dark stripes which are curled edges of those MgO flakes (highlighted by a white arrow). The AuPd also agglomerated after reuse, especially in AuPd/MgO(3) (compare c & f). The scale bars represent 50 nm.

X-ray photoelectron spectroscopy (XPS) analysis of the AuPd/MgO catalysts is challenging due to the overlap of the Pd(3d)/Au(4d) region with the Mg KLL Auger structure and also the overlap of the Mg(2s) region with the Au(4f) photoemission peaks. Nevertheless, by comparison with similarly treated unsupported MgO samples, we can be confident of the Mg(2s)/Au(4f) fitting which reveals solely metallic gold (binding energy (BE) 83.5 eV) in all samples. However the apparent concentration is markedly different in each sample (see figure 9 (a)) and can be related to the dispersion of the Au on the MgO surface. We cannot confidently determine the surface Pd concentration in all samples. However for those where we can fit a derived Auger line shape (obtained from standard reference materials)³⁷ together with the Pd signal (supporting information Figure S6), we note that the Pd is metallic as reflected by the binding energy (~ 334.5 eV). In respect of the MgO supports, for all but AuPd/MgO(3)-MIm prepared catalysts, the support is comprised of primarily hydroxide, although trace carbonate is present on all surfaces. The AuPd/MgO(3)-MIm catalyst comprises of a much higher carbonate component (verified by a corresponding C(1s) energy at *ca.* 290 eV) and oxide.

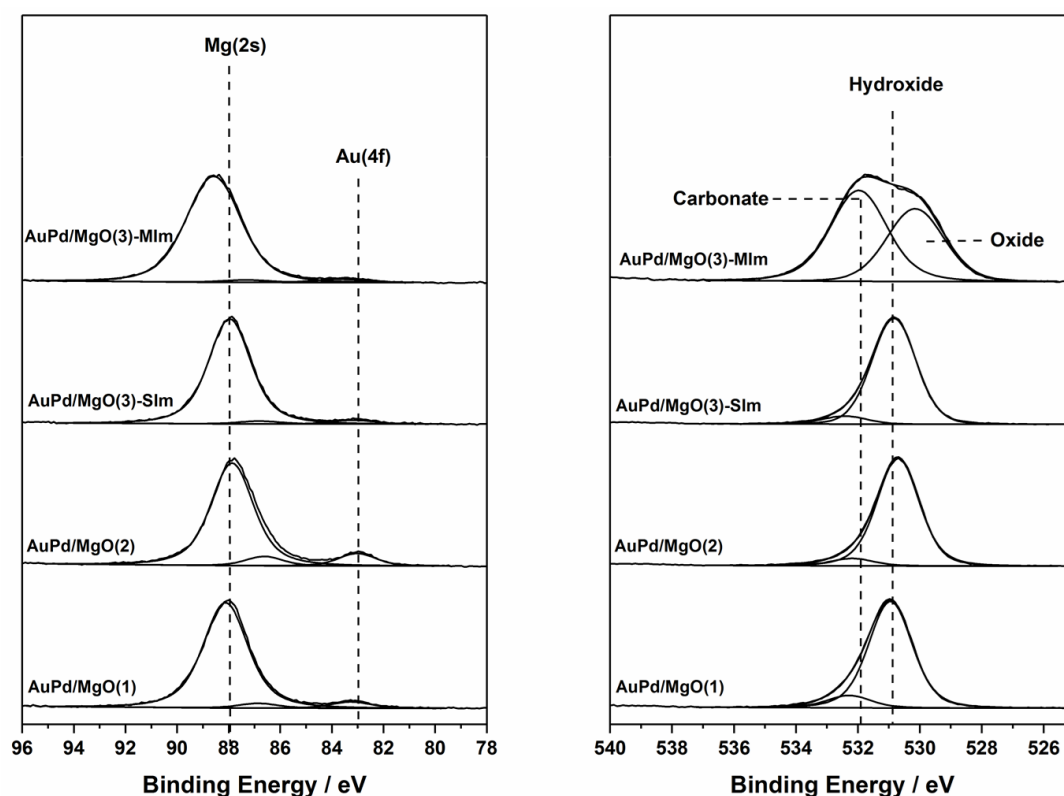


Figure 9. X-ray photoelectron spectra for (a) Mg(2s)/Au(4f) and (b) O(1s) regions for the different fresh AuPd/MgO (X) catalysts where X = 1, 2, 3

A close examination of the XPS data of the fresh and spent AuPd/MgO(3) catalysts and the support material (supporting information Figure S7) reveals that the fresh samples typically comprise of a hydroxide phase, whilst the spent catalyst has a large increase in carbonate species.⁵⁰ Specifically, 1% AuPd/MgO(3) fresh catalyst comprise of Mg(OH)₂ as evidence by the Mg(2s) peak at 88.4 eV and metallic Au (83.3 eV).⁵¹ This correlates well with the XRD data (Figure 6). Again, Au is found in a metallic state (83.7 eV), for the spent catalyst, the shift upwards in energy typically signifying an increase in particle size. Successive uses of this sample result in the laydown of organic oxygenated carbon species on the surface leading to deactivation, as evidenced by the TGA-MS studies, shown in Figure 5.

The above results indicate that all the AuPd/MgO catalysts deactivate during the selective oxidation of benzyl alcohol under liquid phase conditions. Many deactivation pathways including (a) support phase changes from MgO to Mg(OH)₂ and MgCO₃, (b) leaching of MgO support into the reaction mixture, (c) small amount of AuPd leaching, (d) sintering of AuPd nanoparticles, (e) adsorption of reactants and products are active

in this system. Some of the pathways such as AuPd leaching and AuPd sintering could be the result of MgO leaching and phase transformation. Chloride ions are known to contribute to the deactivation of supported metal catalysts and we used excess of chloride ions during the catalyst synthesis. However, no Cl was detected in the AuPd/MgO(3) catalyst through X-ray energy dispersive spectroscopic (XEDS) analysis (supporting information Figure S8). Hence, we propose that Mg leaching and support phase transformation are the major deactivation pathways in this system. It is challenging to identify the most probable pathway because of the difficulty in separating one deactivation pathway with another. Another challenge is the dynamic nature of the support with reversible phase changes. *In situ* spectroscopic methods are necessary to characterise both the support and the metal nanoparticles during the reaction to have a better understanding of the deactivation pathway.

Conclusion

Bimetallic gold-palladium nanoalloy particles were supported on different MgO materials, prepared from different Mg precursors. All these catalysts were tested for the solvent-free selective aerobic oxidation of benzyl alcohol and found to be active and very selective (>97%) to benzaldehyde. Among all the different MgO supports tested, MgO prepared *via* the thermal decomposition of magnesium oxalate (MgO(3)) displayed the highest activity. However, all these catalysts were found to deactivate during the reaction. The mode of deactivation for 1% AuPd/MgO(3) was studied in detail using different characterisation techniques: *in situ* XRD, XPS, ICP-MS, TEM and TGA-MS. From the data, it is clear that MgO undergoes phase changes from MgO to Mg(OH)₂ and MgCO₃ during immobilisation of nanoparticles and during the catalytic reaction, because of the formation of H₂O during the oxidative dehydrogenation reaction. Strong adsorption of reactants and products on the catalyst surface, during the reaction, were also observed. Simple washing with organic solvents and drying did not remove these compounds. The phase change and the adsorption of organic compounds could be reversed through appropriate high temperature heat treatments, however during this process the nanoparticles sinter substantially. Leaching of the support material was also observed during the reaction. Among the three different MgO supports studied in this article, an inverse correlation between the catalytic activity and Mg leaching has been observed. This data further suggests that changing the synthesis methodology of the support can control the leaching properties of MgO.

Based on these evidences, we report that the leaching of support material and sintering of nanoparticles are the reasons for the deactivation of AuPd supported on MgO catalyst. Though MgO is a very good support for selective oxidation reactions, it may not be suitable for liquid phase reactions where water and/or carboxylic acids are involved.

Acknowledgement

HA thanks King Abdulaziz City for Science and Technology (KACST) in Saudi Arabia for financial support. SGM thanks Cardiff University for her PhD studentship. RD thanks the European Union for his Erasmus+ grant to visit Cardiff and acknowledges prof dr.Petra de Jongh for her supervision. EN thanks TU Berlin for her IPODI fellowship. MS and QH thanks Cardiff University for their University Research Fellowships. Authors thank Peter Miedziak of Cardiff Catalysis Institute for TEM measurements and Simon Waller for ICP measurements.

References:

1. T. Mallat and A. Baiker, *Chem. Rev.*, 2004, **104**, 3037-3058.
2. C. H. Bamford, C. F. H. Tipper and R. G. Compton, *Liquid Phase Oxidation*, Elsevier, Oxford, 1980.
3. R. A. Sheldon and J. K. Kochi, *Metal-Catalysed Oxidations of Organic Compounds*, Academic Press, New York, 1981.
4. R. A. Sheldon, *Catal. Today*, 1987, **1**, 351-355.
5. R. A. Sheldon, *Stud. Surf. Sci. Catal.*, 1991, **59**, 33-54.
6. S. Y. Lin and I. S. Lin, *Ullmanns Encyclopedia of Industrial Chemistry*, 1990, 305.
7. G. Centi, F. Cavani and F. Trifirò, in *Selective Oxidation by Heterogeneous Catalysis*, Springer US, Boston, MA, 2001, , pp. 1-24.
8. R. A. Sheldon and H. van Bekkum, in *Fine Chemicals through Heterogeneous Catalysis*, Wiley-VCH Verlag GmbH, 2007, ch09, pp. 473-551.
9. P. Gallezot, *Catal. Today*, 1997, **37**, 405-418.
10. G. J. Ten Brink, I. W. C. E. Arends and R. A. Sheldon, *Science*, 2000, **287**, 1636-1639.

11. R. A. Sheldon, I. W. C. E. Arends, G.-J. ten Brink and A. Dijkstra, *Acc. Chem. Res.*, 2002, **35**, 774-781.
12. M. Hudlicky, *Oxidation in Organic Chemistry*, American Chemical Society, Washington DC, 1990.
13. A. Villa, N. Janjic, P. Spontoni, D. Wang, D. Su and L. Prati, *Appl. Catal. A: Gen.*, 2009, **364**, 221-228.
14. S. Marx and A. Baiker, *J. Phys. Chem. C*, 2009, **113**, 6191-6201.
15. M. Caravati, J. D. Grunwaldt and A. Baiker, *Phys. Chem. Chem. Phys.*, 2005, **7**, 278-285.
16. M. Ilyas and M. Saeed, *Int. J. Chem. Reactor Eng.*, 2010, **8**.
17. F. Brühne and E. Wright, in *Ullmann's Encyclopedia of Industrial Chemistry*, Wiley-VCH Verlag GmbH & Co. KGaA, 2000.
18. W. B. Hou, N. A. Dehm and R. W. J. Scott, *J. Catal.*, 2008, **253**, 22-27.
19. P. Dash, N. A. Dehm and R. W. J. Scott, *J. Mol. Catal. A: Chemical*, 2008, **286**, 114-119.
20. N. E. Kolli, L. Delannoy and C. Louis, *J. Catal.*, 2013, **297**, 79-92.
21. M. Sankar, N. Dimitratos, P. J. Miedziak, P. P. Wells, C. J. Kiely and G. J. Hutchings, *Chem. Soc. Rev.*, 2012, **41**, 8099-8139.
22. S. Meenakshisundaram, E. Nowicka, P. J. Miedziak, G. L. Brett, R. L. Jenkins, N. Dimitratos, S. H. Taylor, D. W. Knight, D. Bethell and G. J. Hutchings, *Faraday Discuss.*, 2010, **145**, 341-356.
23. M. Sankar, E. Nowicka, R. Tiruvalam, Q. He, S. H. Taylor, C. J. Kiely, D. Bethell, D. W. Knight and G. J. Hutchings, *Chem-Eur J*, 2011, **17**, 6524-6532.
24. D. M. Meier, A. Urakawa and A. Baiker, *J. Phys. Chem C*, 2009, **113**, 21849-21855.
25. E. Cao, M. Sankar, E. Nowicka, Q. He, M. Morad, P. J. Miedziak, S. H. Taylor, D. W. Knight, D. Bethell, C. J. Kiely, A. Gavriilidis and G. J. Hutchings, *Catal. Today*, 2013, **203**, 146-152.
26. G. L. Brett, Q. He, C. Hammond, P. J. Miedziak, N. Dimitratos, M. Sankar, A. A. Herzing, M. Conte, J. A. Lopez-Sanchez, C. J. Kiely, D. W. Knight, S. H. Taylor and G. J. Hutchings, *Angew. Chem. Int. Ed.*, 2011, **50**, 10136-10139.
27. Y. Cao, X. Liu, S. Iqbal, P. J. Miedziak, J. K. Edwards, R. D. Armstrong, D. J. Morgan, J. Wang and G. J. Hutchings, *Catal. Sci. Technol.*, 2016, **6**, 107-117.

28. P. J. Miedziak, H. Alshammari, S. A. Kondrat, T. J. Clarke, T. E. Davies, M. Morad, D. J. Morgan, D. J. Willock, D. W. Knight, S. H. Taylor and G. J. Hutchings, *Green Chem.*, 2014, **16**, 3132-3141.
29. C. Xu, Y. Du, C. Li, J. Yang and G. Yang, *Appl. Catal. B: Environ.*, 2015, **164**, 334-343.
30. Z. Yuan, J. Wang, L. Wang, W. Xie, P. Chen, Z. Hou and X. Zheng, *Bioresour. Technol.*, 2010, **101**, 7088-7092.
31. V. R. Choudhary and D. K. Dumbre, *Top. Catal.*, 2009, **52**, 1677-1687.
32. Y. Hao, M. Mihaylov, E. Ivanova, K. Hadjiivanov, H. Knözinger and B. C. Gates, *J. Catal.*, 2009, **261**, 137-149.
33. X. Wan, W. Deng, Q. Zhang and Y. Wang, *Catal. Today*, 2014, **233**, 147-154.
34. H. Hattori, *Chem. Rev.*, 1995, **95**, 537-558.
35. K. Shimazu, H. Hattori and K. Tanabe, *J. Catal.*, 1977, **48**, 302-311.
36. M. Verziu, B. Cojocaru, J. Hu, R. Richards, C. Ciuculescu, P. Filip and V. I. Parvulescu, *Green Chem.*, 2008, **10**, 373-381.
37. M. Morad, E. Nowicka, M. Douthwaite, S. Iqbal, P. Miedziak, J. K. Edwards, G. L. Brett, Q. He, D. Morgan, H. Alshammari, D. Bethell, D. W. Knight, M. Sankar and G. J. Hutchings, *Catal. Sci. Technol.*, 2017, **7**, 1928-1936.
38. K. Wilson and A. F. Lee, *Catal. Sci. Technol.*, 2012, **2**, 884-897.
39. P. Paalanen, B. M. Weckhuysen and M. Sankar, *Catal. Sci. Technol.*, 2013, **3**, 2869-2880.
40. J. K. Bartley, C. Xu, R. Lloyd, D. I. Enache, D. W. Knight and G. J. Hutchings, *Appl. Catal. B: Environ.*, 2012, **128**, 31-38.
41. P. Putanov, E. Kis, G. Boskovic and K. Lázár, *Appl. Catal.*, 1991, **73**, 17-26.
42. M. Sankar, Q. He, M. Morad, J. Pritchard, S. J. Freakley, J. K. Edwards, S. H. Taylor, D. J. Morgan, A. F. Carley, D. W. Knight, C. J. Kiely and G. J. Hutchings, *ACS Nano*, 2012, **6**, 6600-6613.
43. X. Guo, Y. Li, R. Shi, Q. Liu, E. Zhan and W. Shen, *Appl. Catal. A-Gen.*, 2009, **371**, 108-113.
44. L.-X. Li, D. Xu, X.-Q. Li, W.-C. Liu and Y. Jia, *New J. Chem.*, 2014, **38**, 5445-5452.
45. N. Dimitratos, J. A. Lopez-Sanchez, D. Morgan, A. F. Carley, R. Tiruvalam, C. J. Kiely, D. Bethell and G. J. Hutchings, *Phys. Chem. Chem. Phys.*, 2009, **11**, 5142-5153.

46. M. Morad, M. Sankar, E. Cao, E. Nowicka, T. E. Davies, P. J. Miedziak, D. J. Morgan, D. W. Knight, D. Bethell, A. Gavrilidis and G. J. Hutchings, *Catal. Sci. Technol.*, 2014, **4**, 3120-3128.
47. G. J. Hutchings and C. J. Kiely, *Acc. Chem. Res.*, 2013, **46**, 1759-1772.
48. M. Argyle and C. Bartholomew, *Catalysts*, 2015, **5**, 145.
49. J. A. Moulijn, A. E. van Diepen and F. Kapteijn, in *Handbook of Heterogeneous Catalysis*, Wiley-VCH Verlag GmbH & Co. KGaA, 2008,
50. J. M. Montero, M. A. Isaacs, A. F. Lee, J. M. Lynam and K. Wilson, *Surf. Sci.*, 2016, **646**, 170-178.
51. M. Murdoch, G. I. N. Waterhouse, M. A. Nadeem, J. B. Metson, M. A. Keane, R. F. Howe, J. Llorca and H. Idriss, *Nat. Chem.*, 2011, **3**, 489-492.